



# Comparison of different approaches to modelling the fishtail shape in RE-123 bulk superconductors

M. Jirsa<sup>a,b,\*</sup>, M.R. Koblischka<sup>b,c</sup>, T. Higuchi<sup>b</sup>, M. Muralidhar<sup>b</sup>, M. Murakami<sup>b</sup>

<sup>a</sup> *Institute of Physics, ASCR, Na Slovance 2, CZ-182 21 Praha 8, Czech Republic*

<sup>b</sup> *Superconductivity Research Laboratory, ISTEC, Division 3, 1-16-25 Shibaura, Minato, Tokyo 105-0023, Japan*

<sup>c</sup> *Nordic Superconductor Technologies A/S, Priorparken 878, DK-2605 Brøndby, Denmark*

Received 6 March 2000; accepted 10 March 2000

## Abstract

We analyse and compare properties of different models proposed so far for modelling the shapes of  $F(B)$  and  $J(B)$  curves measured in RE-Ba<sub>2</sub>Cu<sub>3</sub>O<sub>7- $\delta$</sub>  (RE-123, RE = rare earth) samples. The formulas following from the discussed models allow for a direct fit of experimental data in various representations. The models divide in two categories, according to the pinning potential used, namely the power-law and the logarithmic potential. We show that none of the pinning regimes proposed for low- $T_c$  superconductors accounts for the fishtail effect (FE) observed in high- $T_c$  materials. The conventional expressions allow a good fit of high- $T_c$  experimental data, however, the resulting fitting parameters are much higher than those predicted by the theory. The logarithmic pinning potential justified in high- $T_c$  materials by both magnetic and transport experiments leads to  $F(B)$  and  $J(B)$  functions that decay exponentially at high fields. The fit of experiments on a wide range of RE-123 samples, using only one free parameter, is nearly perfect. The role of free parameters is discussed in all the models. © 2000 Elsevier Science B.V. All rights reserved.

PACS: 74.60 Ec; 74.60 Ge; 74.60 Jg

Keywords: RE-Ba<sub>2</sub>Cu<sub>3</sub>O<sub>7- $\delta$</sub> ; Fishtail effect; Rare earth

## 1. Introduction

Although the understanding of physical background of the critical current enhancement at high fields (peak or fishtail effect, FE) is still incomplete, FE has gained a significant importance in bulk applications of high- $T_c$  superconductors. Economical aspects of such applications like superconducting per-

manent magnets, fly wheels, bearings, superconducting motors etc. put strong demands on the physical properties of materials in use. Critical currents are required to be as high as possible, especially at high fields.

Numerous explanations have been proposed for this phenomenon, as a matching effect, a field induced granularity, field induced pinning site activation (e.g. due to  $T_c$  fluctuations, so called  $\Delta\kappa$ - or  $\Delta T_c$ -effect), field dependent creep effects, crossover of pinning regimes or a phase transition in vortex matter. The appearance of a secondary peak on magnetisation curve reflects rather complex interaction of the operative pinning structure with the actual

\* Corresponding author. Czech Academy of Sciences, Institute of Physics, ASCR, Na Slovance 2, CZ-182 21 Praha 8, Czech Republic. Tel.: +420-2-6605-2718; fax: +420-2-821227.

E-mail address: jirsa@fzu.cz (M. Jirsa).

vortex matter and this allows a wide field for speculations.

Anyway, the question of a relevant pinning structure becomes now more transparent. A series of experiments on differently oxygenated clean  $\text{YBa}_2\text{Cu}_3\text{O}_{7-\delta}$  single crystals has identified the appearance of FE with existence of randomly distributed oxygen-deficient zones in the sample [1–7]. A similar conclusion was also drawn for clean  $\text{NdBa}_2\text{Cu}_3\text{O}_{7-\delta}$  single crystals [8]. Angular measurements of an induced magnetic moment in different RE-123 compounds gave evidence that the specific FE shape is there related to the vortex pinning by an *isotropic uncorrelated pinning disorder*. Though the principal source of pinning in RE-123 materials are most probably oxygen vacancies, a similar role can most probably play also fine particles of RE-211 or RE-422 phases [9–12], Nd-rich clusters [13,14] or other imperfections of an appropriate size.

The works of Küpfer et al. [3,4], Nishizaki et al. [5–7] and others dealt with a weak pinning disorder in clean Y-123 single crystals. These studies gave evidence of a rich structure of the  $B$ – $T$  phase diagram close to irreversibility line. In the framework of these studies the secondary peak appears on the border between zones of a relatively weakly pinned vortex lattice and a vortex glass that much better accommodates to the pinning structure and is, therefore, better pinned. The low-field slope of the peak (the increase of pinning with field) is thus attributed to the crossover between these two regimes. A similar behaviour has been also observed on Bi-2212 single crystals [15,16] and other compounds. A strong pinning disorder, resulting in RE-123 materials in the famous fishtail peak, follows probably a similar scenario. Only the phase diagram is simpler, with a monotonous decay of the peak effect with increasing temperature up to  $T_c$  and without any re-entrant behaviour [3,4].

The knowledge of the principal pinning agent and the vortex phase diagram related to the peak effect in RE-123 are certainly basic for understanding the field and temperature dependencies of this phenomenon. However, a microscopic theory that would correlate characteristic empirical parameters with microscopic properties is still missing. This theory would enable the material characterisation and might

help in identification of more effective pinning mechanisms for enhancement of critical currents and irreversibility field.

In this paper, we restrict ourselves to the strong pinning disorder. We compare several models used in the analysis of magnetic and transport data in superconductors, with a special attention to the description of FE in RE-123 materials. We hope this analysis may help in development of a satisfactory model that would fully explain the empirical behaviour of macroscopic magnetic quantities in terms of microscopic processes active at different stages of the sample magnetization.

## 2. Classical pinning theories

The classical theories usually solved the case of a rigid or slightly elastically bound vortex lattice. Relaxation phenomena were mostly omitted as not substantial for conventional superconductors. Interaction between the vortex lattice and the system of pinning defects was treated in terms of the pinning force density,  $F = BJ$ , where  $B$  is the applied field and  $J$  the critical current density. It was empirically found [17,18] that most experimental data in conventional superconductors, expressed in terms of  $F(B)$ , scale with field and temperature as

$$F(B) \propto B_{c2}^r b^p (1 - b)^q, \quad (1)$$

where  $b = B/B_{c2}$  and  $r$ ,  $p$ , and  $q$  are positive empirical parameters reflecting the microstructure features of the material. Kramer [18] proposed a model explaining the peak in  $F(B)$  dependence by a crossover from the regime individual vortex pinning at low fields to the regime of an elastically interacting vortex lattice at high fields.

For testing the scaling property with temperature and field, it is useful to write the Kramer's law in a normalized form. It is easy to show that the peak position  $B_{fp}$  and the upper critical field  $B_{c2}$  are interrelated by factor  $p/(p + q)$ , thus Eq. (1) can be expressed as

$$F_n = \frac{(p + q)^{p+q}}{p^p q^q} b^p (1 - b)^q, \quad (2)$$

or, in terms of  $b_{fp} = B/B_{fp}$ , as

$$F_n = b_{fp}^p \left[ 1 + \frac{p}{q} (1 - b_{fp}) \right]^q. \quad (3)$$

Analogous expressions for the normalized current density  $j_n$  can be simply obtained by replacing  $p$  by  $p - 1$  in the above equations. Note that while  $F_n(B)$  exhibits maximum even for  $0 < p \leq 1$ ,  $j_n(B)$  continuously decreases with increasing field for  $p \leq 1$ . Thus only  $p$  values higher than 1 are relevant for the fishtail shape, which excludes most of the previously treated situations [19–22] from the consideration in high- $T_c$  superconductors [23]. Only two cases from those theoretically studied so far can produce a maximum on the  $J(B)$  curve: The pinning by superconductive point- and surface-defects [19] (so called  $\Delta\kappa$  pinning), with  $p = 1.5$  and  $p = 2$ , respectively. However, these peaks have steep high-field slopes at  $B_{c2}$  (the derivatives being  $-2.6$  and  $-4$  at  $B_{c2}$ , respectively), and do not resemble the FE shape observed in RE-123 materials where the  $j_n(B)$  is usually at high fields strongly depressed.

As the course of both  $F(B)$  and  $J(B)$  dependencies is at high fields controlled mainly by the term  $(1 - b)^q$ , the derivative of which at  $B \rightarrow B_{c2}$  is zero for  $q > 1$ , finite for  $q = 1$ , and becomes infinite for  $q < 1$ , only  $q > 1$  is relevant to the FE shape experimentally observed in RE-123. This is manifested by Fig. 1 where  $j_n(b)$  dependencies according to Eq. (2) (with  $p$  replaced by  $p - 1$ ) are shown for  $p = 2$  and  $q$  varying between 0.2 and 4. Evidently, for this  $p$

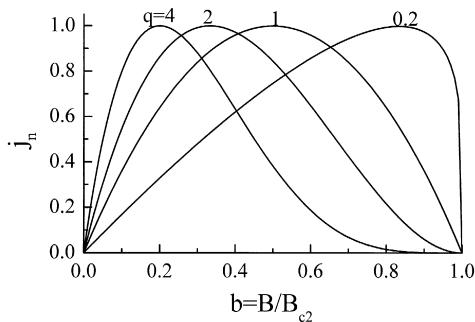


Fig. 1. The normalized  $j_n(b)$  curves,  $b = B/B_{c2}$ , according to Eq. (2), with  $p - 1 = 1$  instead of  $p$ , and  $q$  varying from 0.2 to 4. Only the curves with  $q > 2$  resemble the experimental FE curves observed in RE-123 materials.

value the typical fishtail shape is well reproduced by  $q \geq 2$ . A  $p$  value increased above 2 shifts the peak to even higher fields, which requires also a higher  $q$  value to fit the experimental data. We conclude that the use of the Kramer's scaling law (1) in the analysis of a fully developed fishtail effect in RE-123 materials requires rather high values of the parameters  $p$  and  $q$  that miss so far a theoretical explanation.

For fitting experimental data with Kramer's law it is remarkable that the relative position of FE maximum with respect to  $B_{c2}$  is controlled by both parameters  $p$  and  $q$ , and the same applies for the curve width.

If the peak positions on both  $J(B)$  and  $F(B)$  curves,  $B_p$  and  $B_{fp}$ , respectively, and also  $B_{c2}$  are experimentally accessible, the  $F_n(B)$  and  $j_n(B)$  curves can be modelled using the  $p$  and  $q$  values determined analytically as

$$p = \frac{B_{fp}}{B_{c2}} \frac{B_{c2} - B_p}{B_{fp} - B_p}; \quad q = \left( 1 - \frac{B_{fp}}{B_{c2}} \right) \frac{B_{c2} - B_p}{B_{fp} - B_p}. \quad (4)$$

### 3. Recent models based on a power-law potential

Yeshurun and Malozemoff [24] pointed out that the thermally activated giant flux creep in HTSC results in the critical current disappearance at the irreversibility field  $B_{irr}$  instead of  $B_{c2}$ . The authors concluded that the activation energy per vortex becomes limited by flux line spacing  $d$  ( $\ll \lambda$ ). This leads to the field dependence of the activation energy  $U_0 \propto B^{-1}$  or  $U_0 \propto B^{-3/2}$  for the activation volume limited in the direction along the vortices by  $\xi$ , the superconductive coherence length, or  $d$ , respectively. In contrast to classical theories,  $U_0$  decreases at high fields as a power of field.

Fabricatore et al. [25] modified the classical approach by using as a field reference the empirical value  $B_{irr}$  instead of  $B_{c2}$ . Alternatively, the authors assumed the two cases suggested by Yeshurun and Malozemoff,  $V \propto d^3$  and  $V \propto d^2 \xi$ , and derived an analytical relation between  $B_{irr}$  and  $B_{c2}$  for these two cases. In accordance with Ref. [24] they re-

stricted themselves to the Anderson–Kim current regime and arrived in this case at the expression

$$F \propto b_i^\gamma (1 - b_i^\epsilon), \quad (5)$$

with  $\epsilon = 1.5 - \gamma$  for the activation volume  $V = d^3$  and  $\epsilon = 1 - \gamma$  for  $V = d^2\xi$ . If we apply the extreme condition onto relation (5), we get

$$F_n(b_i) = \left( \frac{\epsilon + \gamma}{\gamma} \right)^{\gamma/\epsilon} \frac{\epsilon + \gamma}{\epsilon} b_i^\gamma (1 - b_i^\epsilon). \quad (6)$$

For the  $\text{Bi}_2\text{Sr}_2\text{CaCu}_2\text{O}_{10}$  (Bi-2212) samples studied in Ref. [25] none of the cases  $\epsilon = 1.5 - \gamma$  and  $\epsilon = 1 - \gamma$  gave a good fit of the experimental data.

If  $\epsilon$  and  $\gamma$  would be left as free parameters, then Eq. (6) serves a similar possibility to fit experimental data as the classical Eq. (2). Note that we can identify  $\gamma$  with  $p$ , which implies that for an appearance of the fishtail maximum  $\gamma$  has to be higher than 1.

To extend the model over the Anderson–Kim’s critical currents regime, Fabricatore et al. used the empirically found relation between electric field and critical current density in the superconductor. This relation implied the use of another type of pinning potential. This extension is therefore out of the scope of this chapter and will be discussed in the next section.

A comprehensive study of the flux dynamics in high- $T_c$  materials was made by Yin et al. [26,27]. Besides relaxation effects the authors took also into account the energy dissipation due to viscous forces acting on the moving vortices. The  $F(B)$  dependence derived in Ref. [27] for a high- $T_c$  superconductor in critical state can be written in a close form as

$$F(b_i) = \alpha'(T) b_i^{s+1} (C - b_i)^q (1 - \zeta b_i^{-s} \beta^q)^{3\nu} \times [1 - \zeta b_i^{-s} \beta^q + E_c / (\rho_n J_{c0} b)], \quad (7)$$

where  $\alpha'(T) = \alpha(T) C^{-q} (C - 1)^q B_{\text{irr}}^{s+1}$ ,  $C = B_{c2}/B_{\text{irr}}$ ,  $b_i = B/B_{\text{irr}}$ ,  $\zeta = \alpha(T)/\alpha(T_{\text{irr}}(B))$ ,  $\beta = (C - 1)/(C - b_i)$ ,  $b = B/B_{c2}$ ,  $T_{\text{irr}}(B)$  is the irreversible temperature for the field  $B$ ,  $\rho_n$  is the normal resistivity,  $E_c$  is the limiting criterion set on the electrical field,  $J_{c0}$  is the critical current density in absence of flux creep,  $s$ ,  $q$ , and  $\nu$  are empirical parameters, and

$\alpha(T)$  is the temperature-dependent factor from the empirical Ansatz

$$U_0(T, B) = \alpha(T) B^s (1 - b)^q. \quad (8)$$

Formula (7) consists of one term increasing with a power of  $B$  (for positive  $s$ ) and three terms decreasing at different rates with increasing  $B$ . Such a function develops a maximum at an intermediate field  $B_{\text{fp}}$ . For  $s \geq 1$  and  $q \geq 2$  and for  $B \leq 0.9 B_{\text{irr}}$ , the product of the last two brackets in Eq. (7) equals 1, up to a few percent. This product drops fast to zero only above  $0.9 B_{\text{irr}}$  where the rest of the expression is already small. We can therefore write an approximate relation

$$F(b) = \alpha'(T) C^{1+s+q} b^{s+1} (1 - b)^q. \quad (9)$$

We see that the Yin’s approach results in a scaling relation very similar to the classical Kramer’s law. The effect of creep is included in the parameter  $C$ . By identifying  $p$  with  $s + 1$  all conclusions regarding the classical model can be used also for this approximation. As  $C$  is field-independent, the approximate normalized pinning force density,  $F_n(b)$ , is expressed by the classical Eq. (2). To reflect the experimental fact that the critical current disappears at the irreversibility field,  $B_{\text{irr}}$ , the applied field should be reduced to  $B_{\text{irr}}$ . This can be accomplished by replacing  $b$  by  $b_i/C$ . The factor  $C$  can be determined experimentally or used as an additional free parameter for fitting. A normalized critical current density  $j_n(b_i)$  can be derived from Eq. (2) by replacing  $p$  by  $s$ , and, as above,  $b$  by  $b_i/C$ .

The parameters  $s$  and  $q$  can be again determined analytically using formula (4) with  $p$  replaced by  $s + 1$ . Besides  $B_p$ ,  $B_{\text{fp}}$ , and  $B_{c2}$  values needed for determination of  $s$  and  $q$ ,  $B_{\text{irr}}$  is also required for the estimation of  $C$ .

#### 4. Models based on a logarithmic potential

Fabricatore et al. [25] explored the relation commonly found in transport measurements,

$$J = J_0 \left( \frac{E}{E_0} \right)^{kT/U_0}, \quad (10)$$

which can be translated into the logarithmic dependence  $U_{\text{eff}} \propto \ln(J/J_0)$ . In the derivation of  $F(B)$  dependence only low field region was considered, where, following the classical approach,  $F_{p0}$ , the ideal pinning force density without thermal activation, was approximated by a power of field,  $B^\gamma$ . The authors obtained a rather complicated expression<sup>1</sup>

$$F(b_i) = R_3 b_i C^{b_i^\epsilon}, \quad (11)$$

with  $R_3 = J_0 B_{\text{irr}}$ ,  $b_i = B/B_{\text{irr}}$ ,  $C = (E/E_0)^{\ln(J_{\text{irr}}/J_0)/\ln(E/E_0)}$ , and  $\epsilon = 1.5 - \gamma$  for the activation volume  $V = d^3$  and  $\epsilon = 1 - \gamma$  for  $V = d^2 \xi$ .

Eq. 11 in a normalized form is much more transparent (see Appendix A),

$$F_n(b_{\text{fp}}) = b_{\text{fp}} \exp\left[(1 - b_{\text{fp}}^\epsilon)/\epsilon\right], \quad (12)$$

with  $F_n = F/F(B_{\text{fp}})$  and  $b_{\text{fp}} = B/B_{\text{fp}}$ . The field scale  $B_{\text{irr}}$  can be introduced in Eq. (12) by replacing  $b_{\text{fp}}$  by  $b_i/b_{\text{fi}}$  where  $b_{\text{fi}} = B_{\text{fp}}/B_{\text{irr}}$ . In Ref. [25], a satisfactory fit of the transport experimental data in the Bi-2212 sample in fields below  $0.4 B_{\text{irr}}$  was achieved with this formula with  $\epsilon = 1.5 - \gamma$  and  $b_{\text{fi}} = 0.16$ . However, the linear field dependence of the factor standing before the exponential function in Eq. (12) implies that the corresponding  $J(B)$  dependence is a decreasing function of field in the whole field range and thus does not exhibit any fishtail maximum. Therefore, this model in its original form is inappropriate for interpretation of FE data in RE-123 materials.

Another approach using logarithmic pinning potential was chosen by Perkins et al. [28]. The authors treated a general thermally activated creep process, described by the classical formula

$$E = B\nu x \exp\left(\frac{U_{\text{eff}}}{kT}\right), \quad (13)$$

where  $E$  is the electric field in the sample associated with the magnetic induction during an applied field sweep,  $B$  is the applied magnetic field,  $\nu$  is the attempt frequency,  $x$  is the mean vortex hop distance,  $U_{\text{eff}}$  is the effective energy barrier for ther-

mally activated jumps, and  $J$  is the critical current density. The authors considered  $U_{\text{eff}}$  to be a function of  $T$ ,  $B$ , and  $J$ , written in the form

$$U_{\text{eff}}(T, B, J) = U_0(T, B) V[J/J_0(T, B)], \quad (14)$$

where  $U_0$  and  $J_0$  are characteristic energy and current scales, respectively, and  $V(J/J_0)$  is a function describing the current dependence  $U_{\text{eff}}(J)$ . It was pointed out that the empirically found scaling of the magnetic hysteresis loop (MHL) with the electric field  $E$  implies that the characteristic scales of  $J$  and  $U_{\text{eff}}$  are power-law functions of the applied field,  $J_0 \propto B^m$  and  $U_0 \propto B^{-n}$ ,  $m > 0$  and  $n > 0$ . The analysis of the magnetic measurements on Tm-123 showed [28,29] that the function  $V(J/J_0)$  was logarithmic. As mentioned above, the logarithmic  $U_{\text{eff}}(J)$  dependence is in accord with the power-law relation  $J/J_0 = (E/E_0)^\beta$  commonly deduced from transport experiments.

The logarithmic potential causes the critical current density to decay in high fields exponentially with increasing field [28],

$$J \propto B^m \exp(cB^n), \quad (15)$$

where  $c$  is a field independent parameter. Formula (15) exhibits the characteristic peak, with the maximum  $J_{\text{max}}$  at the field  $B_p$ . From the condition for extreme we get [30]  $c = -(m/n)B_p^{-n}$  and

$$j_n(b_p) = b_p^m \exp\left[(1 - b_p^n)m/n\right]. \quad (16)$$

The same expression with the field reduced to  $B_{\text{irr}}$  reads

$$j_n(b_i) = (b_i/b_{\text{pi}})^m \exp\left\{\left[1 - (b_i/b_{\text{pi}})^n\right]m/n\right\}, \quad (17)$$

where  $b_i = B/B_{\text{irr}}$  and  $b_{\text{pi}} = B_p/B_{\text{irr}}$ ;  $b_i/b_{\text{pi}} = b_p$ .

For pinning force density similar expressions can be derived by replacing  $m$  by  $m + 1$ . Of course, a respective peak position,  $B_{\text{fp}}$ , replaces  $B_p$ .

Note that  $B_{\text{irr}}$  is usually defined by means of a criterion for the threshold, behind which either  $J$  or  $F$  becomes negligible. Therefore, the value of  $B_{\text{irr}}$  slightly depends on the chosen experimental method.

<sup>1</sup> There is a misprint in Eq. (26) of Ref. [16]. Here we present the correct result, as derived in the Appendix A.

As shown in Ref. [31],  $m$  can be set equal to 1 for most RE-123 single crystals. Then  $n$  remains the only free parameter. The additional factors  $b_{pi}$  or  $b_{fi} = B_{fp}/B_{irr}$  can be at high temperatures determined experimentally. At low temperatures, where  $B_{irr}$  is out of the experimental field range, these parameters can be used as free to fit the measured part of the MHL. Then, using the fit values of  $b_{pi}$  and/or  $b_{fi}$ ,  $B_{irr}$  can be estimated. In Fig. 2(a) and (b), sets of theoretical  $F_n(b_i)$  and  $F_n(b_{fp})$  curves are presented, according to Eqs. (16) and (17), respectively, with  $n$  replaced with  $n + 1$  and  $B_p$  with  $B_{fp}$ .  $m$  was set equal 1 and  $n$  had the values 0.5, 1, 2, and 3. The respective values of  $b_{fi}$  were 0.065, 0.17, 0.33, and 0.43. The range of the  $n$  values was chosen in accordance with the values deduced from experiments found in literature [31] and  $B_{irr}$  was defined by the criterion  $F_n(B_{irr}) = 2 \times 10^{-3}$ . In Fig. 2(c) and (d), the corresponding  $j_n(b_i)$  [Eq. (16)] and  $j_n(b_p)$  [Eq. (17)] dependencies are shown.  $B_{irr}$  in Fig. 2(c) is defined by the criterion  $j_n = 2 \times 10^{-3}$ . For  $n =$

0.5, 1, 2, 3, and 4 we get  $b_{pi} = 0.035, 0.115, 0.255, 0.355,$  and  $0.44,$  respectively.

In this model only  $n$  controls the FE peak positions  $B_{fp}$  and  $B_p$  with respect to  $B_{irr}$ . For  $F_n(b_i)$  and  $j_n(b_i)$  dependencies, the higher  $n$ , the closer is the fishtail maximum to the irreversibility field and the wider is the curve [see Fig. 2(a) and (c)]. The  $F_n(b_{fp})$  and  $j_n(b_p)$  curves are in the contrary narrower for higher  $n$  (see Fig. 2(b) and (d)). Evidently,  $n$  can serve as a measure of the curve width and, therefore, for characterisation purposes.

Starting from the relation  $B_{fp}/B_p = [(m + 1)/m]^{1/n}$  (see Ref. [31]) and assuming  $m = 1$ , we get

$$n = \ln 2 / \ln(B_{fp}/B_p). \quad (18)$$

The fact that only the peak positions  $B_p$  and  $B_{fp}$  are needed for determination of  $n$  and, consequently, of the shape of the whole curve up to  $B_{irr}$ , is a big advantage of this model. Peak positions, lying usually below  $0.5 B_{irr}$ , are accessible in a much wider

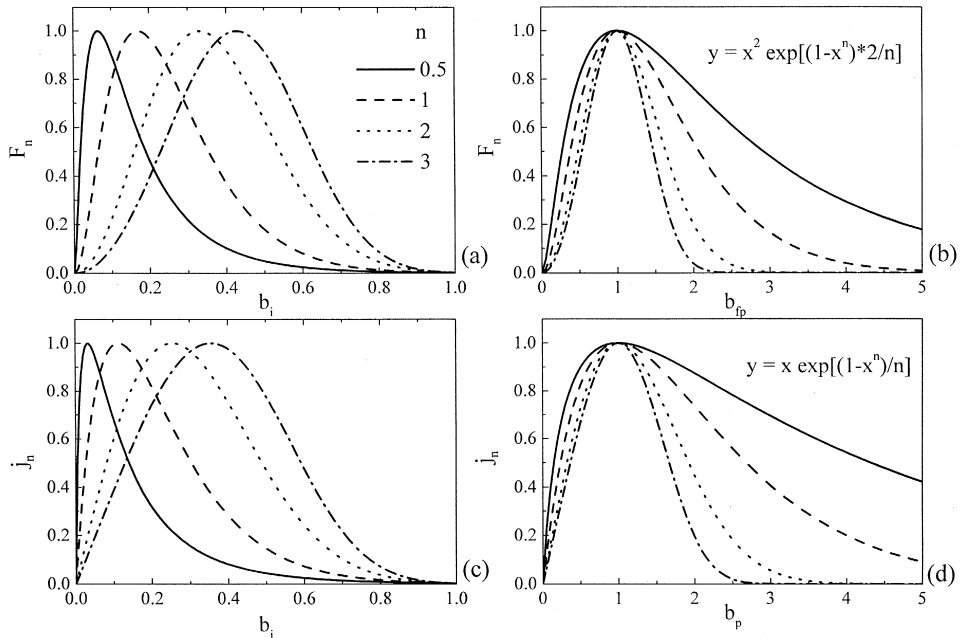


Fig. 2. (a) The theoretical  $F_n(b_i)$  curves,  $b_i = B/B_{irr}$ , according to Eq. (17) with  $m + 1$  instead of  $m$ . The  $B_{irr}$  value was defined by the criterion  $F_n(1) = 0.002\%$ . (b) The  $F_n(b_{fp})$  curves,  $b_{fp} = B/B_{fp}$ , according to Eq. (16) with  $m + 1$  instead of  $m$  and the same values  $n$  as indicated in (a). (c) The  $j_n(b_i)$  curves corresponding to Fig. 4(a) (Eq. (17)) with  $m = 1$ . The  $B_{irr}$  value was defined by the criterion  $j_n(1) = 0.003$ . (d) The curves  $j_n(b_p)$ ,  $b_p = B/B_p$ , according to Eq. (16). The parameters  $m$  and  $n$  are the same in all four figures,  $m = 1$  and  $n$  varying from 0.5 to 3.

temperature range than  $B_{\text{irr}}$  and/or  $B_{c2}$  needed in the previous models. Knowing  $n$ , the  $B_{\text{irr}}$  value can be also deduced.

## 5. Comparison of the models

### 5.1. General remarks

In general, the models discussed above can be divided into two groups, according to the type of pinning potential in use. The models with the power-law potential produce field dependencies of  $J$  and  $F$  decreasing at high fields as a power of  $(1 - \alpha B)$ , where  $1/\alpha$  is an appropriate field scale. The models using the logarithmic pinning potential exhibit an exponential decay at high fields.

Irrespective of the model, all theoretical  $J(B)$  and  $F(B)$  dependencies discussed in this paper are products of one term increasing as a power of  $B$  and another term decaying with increasing field. If we consider these formulas as fitting functions, we can identify the parameter  $m$  from the Perkins' model with the factor  $p - 1$  in the classical models, with  $\gamma$  in the Fabricatore's power-law model, Eq. (5), with  $s$  in the Yin's model, so that the terms increasing with field are same in all the models.

As concerns the second term, decreasing with field, we can identify the Fabricatore's parameter  $\varepsilon$  from Eq. (12) with the  $n$  from Eq. (16). With  $m = 0$ , the expressions for the normalized pinning force density are in both models formally identical. However, the zero value of  $m$  in Eq. (12) means that  $J_0$  is field-independent in this Fabricatore's model, which is incompatible with RE-123 bulk samples, where  $m \approx 1$  is usually found. Also, the above suggested equivalence of  $n$  and  $\varepsilon$  makes the analysis of experiments on RE-123 samples difficult. The majority of  $n$  values established experimentally in RE-123 lie around 1.5 or at least above 1, which implies  $\gamma \leq 0$ . This is in contradiction with present theories of elastic interactions in a vortex lattice. Here we have to bear in mind that the similarity of these two approaches is only formal and cannot be taken strictly.

The Yin's model in its original, complete form, Eq. (7), includes besides the principal two free pa-

rameters,  $s$  and  $q$ , also a number of additional empirical factors. As shown above, this expression can be significantly simplified, which eliminates most of the additional parameters from the fitting procedure. Only the factors  $s$ ,  $q$ , and  $C = B_{c2}/B_{\text{irr}}$  remain. The latter parameter enables to normalize the field variable to the empirical value of  $B_{\text{irr}}$  instead of  $B_{c2}$ . If the  $B_{c2}$  value is not available,  $C$  can be taken as an additional free parameter. Using the given values  $s = 1.88$  and  $q = 4.21$  and the normalized peak position from Fig. 2 of Ref. [27], we deduced from Eq. (9)  $C = 1.08$ .

None of the models discussed in this paper reproduces the experimentally observed minimum on the  $j_c(B)$  curve at low fields. According to Ref. [30], we believe that this minimum results from overlapping of two contributions, one due to interaction of vortex matter with the actual pinning structure and another one due to self-fields. The latter contribution is obviously restricted to low field region, it decays exponentially with field [30], similarly as  $j_c(B)$  in samples without peak effect [32–35]. The different characters of both contributions are manifested by quite different scaling with temperature and angle of field with respect to the  $c$ -axis.

### 5.2. Comparison of the fit quality

The fit quality of the models with the power-law and the logarithmic potential is compared in Fig. 3 on magnetic data of three different RE-123 single crystals. While the first two sets of experimental data were reconstructed from literature, the last set was measured by us in ISTE. The data were chosen that do not show any effect of twin plane pinning. For the Tm-123 this feature seems to be intrinsic. The Y-123 data were taken at rather high temperatures where the effect (if any) was already negligible. In the melt-textured NEG, the twins were hardly observable. In all three cases the field is normalized to the respective peak position in both the  $F(B)$  and  $J(B)$  representation. The  $F(B)$  data (Fig. 3(a), (c), (e)) were fitted by means of Eqs. (2) and (16) with  $m = 1$  and  $n$  replaced by  $n + 1$ , the  $J(B)$  data (Fig. 3(b), (d), (f)) were analysed using Eq. (2) with  $p$  replaced by  $p - 1$  and Eq. (16). Although the fit quality with both expressions was comparable, the fit

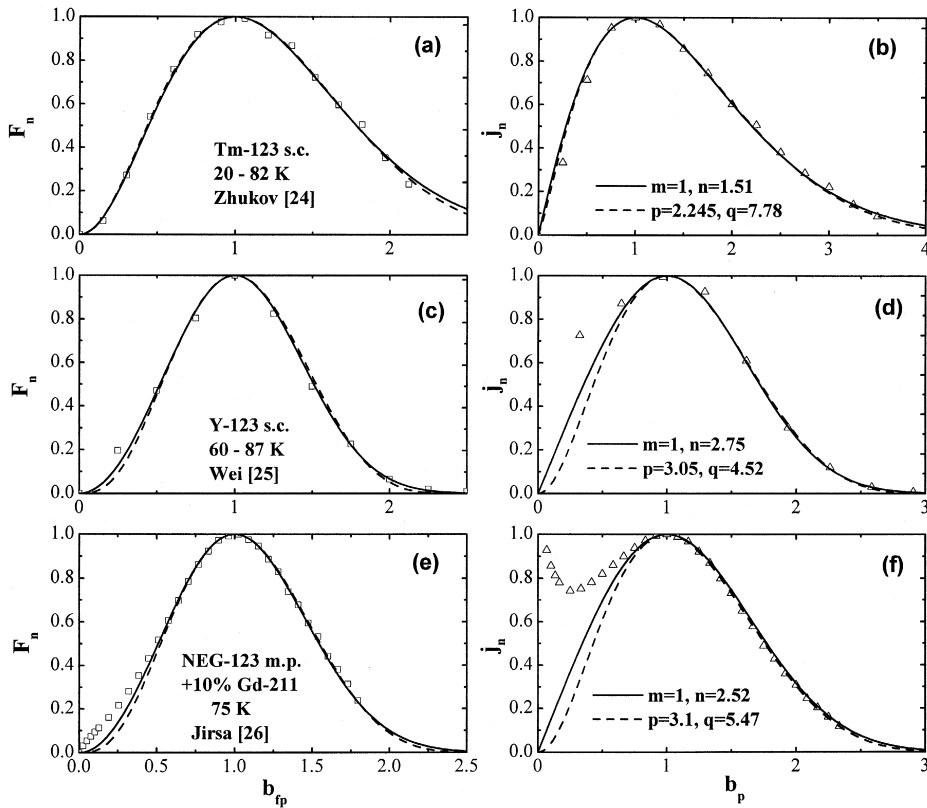


Fig. 3. The fits of the experimental data measured on (a) and (b) a Tm-123 single crystal, (c) and (d) a Y-123 single crystal, and (e) and (f) a  $(\text{Nd}_{0.33}\text{Eu}_{0.33}\text{Gd}_{0.33})\text{Ba}_2\text{Cu}_3\text{O}_{7-\delta}$  melt processed sample with an addition of 10% of a finely dispersed Gd-211 phase. The data in the  $F(B)$  representation ((a), (c), and (e)) are fitted by Eqs. (2) and (16) with  $m$  replaced by  $m + 1$ , the  $J(B)$  dependencies ((b), (d), and (f)) are fitted by Eqs. (2) and (16) with  $p - 1$  set for  $p$ .

with the classical formula was more difficult due to a larger “freedom” of the parameters  $p$  and, espe-

cially,  $q$ . A small change of  $p$  caused quite a large change in  $q$  with nearly unchanged fit quality. This

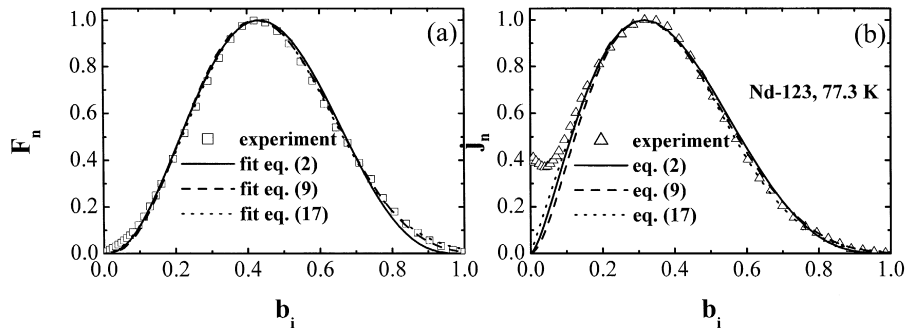


Fig. 4. The fit of the experimental data measured on the Nd-123 single crystal, in (a)  $F(B)$  and (b)  $J(B)$  representation. The applied field is normalised to  $B_{irr}$ . The  $F(B)$  curves were fitted by Eqs. (2), full line; Eq. (9), dashed line; and Eq. (16) with  $m + 1$  instead of  $m$ , dotted line, the  $J(B)$  data were fitted by Eq. (2) with  $p - 1$  set for  $p$ , solid lines; Eq. (9) with  $s$  set for  $s + 1$ , dashed lines; and Eq. (17), dotted lines. The fitting parameters are reported in the text.

means that aside material characteristics and temperature effects also the fitting function itself introduced a significant ambiguity into the fit.

In Fig. 4, we compare fits using three different approaches, the classical theory, Eq. (2), the Yin's formula, Eq. (9), and the model with the logarithmic potential, Eq. (16). For the comparison, we chose the original magnetic moment data measured by Higuchi et al. [36] on a Nd-123 single crystal as these data were also fitted by Yin et al. [27]. The analysed single crystal was twinned but at 77.3 K, where the data for the analysis were taken, the peak lies below the onset of the typical twin depression and the magnetisation curve is not much affected by the twins. The best fit of the  $F(B)$  data by means of Eq. (17) was obtained with  $m = 1$ ,  $n = 2.57$ , and  $b_{\text{fi}} = 0.43$ , Eq. (2) produced the best fit with  $p = 2.54$ ,  $q = 3.27$ , and  $B_{\text{fp}}/B_{\text{c2}} = 0.437$ , and Eq. (9) with  $s = 1.88$ ,  $q = 4.21$ ,  $C = 1.08$ , and  $b_{\text{fi}} = 0.435$ . We see that all the fits practically overlap. Only at the high-field end the curve according to Eq. (2) is more depressed than the other two functions because it takes  $B_{\text{c2}}$  as a reference instead of  $B_{\text{irr}}$ . The fits of the  $J(B)$  data by the same equations are in all cases also very good and give naturally the same parameter values as in the  $F(B)$  representation. As mentioned above, none of the discussed formulas for the  $j_n(b)$  dependence reproduces the experimentally observed low-field peak caused by a different pinning mechanism (self field effect).

All the empirically found parameters  $p$  and  $q$  are rather high in comparison to those predicted by the classical models, including the  $\Delta\kappa$  pinning. Note that such high values were also observed in other RE-123 samples, e.g. Y-123 single crystals [37–39]. The values of  $n$  deduced from the presented experiments lie also at the upper part of the range observed in RE-123 materials [31]. In the samples with a significant content of Nd this might be due to a pinning enhancement by Nd–Ba clusters [13,14]. However, the examples of other RE-123 specimens, without Nd, show that FE maximum lying at relatively high field with respect to  $B_{\text{c2}}$  or  $B_{\text{irr}}$  might be produced by a properly chosen technological treatment also in these materials.

Let us note that the effect of oxygen reduction starting from the optimum doping shifts the peak to lower field. The emphasis to enhance the peak field

for application purposes is just opposite. The experimental results in different LRE-123 materials (Light Rare Earth) indicate that the strong pinning limit does not necessarily result in a low-field position of the second peak. By a proper technology, the strong pinning limit can be shifted towards high fields and high temperatures in the  $B$ – $T$  plane.

## 6. Conclusions

In the present paper we analyse properties of different models used for modelling the fishtail-like magnetic hysteresis loops and the associated critical currents or pinning force densities in RE-123 materials. The models proposed to date can be in general classified according to the pinning potential in use. The models with a power-law potential result in model functions decaying at high fields as  $(1 - \alpha B)^q$ , the models assuming a logarithmic pinning potential result in  $J(B)$  and  $F(B)$  decreasing at high field as  $\exp(cB^n)$  (as shown above, the factor  $c$  is negative).

In all the models the  $J(B)$  and  $F(B)$  functions increase at low fields with a positive power of  $B$ . The shape of the theoretical curves at intermediate and high fields is in the first group, using the power-law potential, governed by all free parameters (mostly two or three). In the second group, with the logarithmic potential, it is possible to fix the parameter  $m$  at the value 1 and then only one free parameter,  $n$ , governs the shape of the whole curve, up to  $B_{\text{irr}}$ , i.e. the position of the peak with respect to  $B_{\text{irr}}$ , and the width of the curve are given by this single parameter. We note that attempts to fix the power of the term increasing with field in the models using power-law potential were not successful. The fit was always significantly worse than with both parameter free.

In the case of the MHL scaling with temperature, the width of the normalized curve ought to be temperature independent, and the scaling property requires a constant  $n$ . The same conclusion can be drawn for the parameters  $p$  and  $q$ . Here both parameters have to be temperature independent. In the contrary,  $n$ ,  $q$ , or  $p$  varying with temperature indicate an absence of scaling. In the model with logarithmic potential we can deduce from the definition of  $n$  that the existence of scaling is related to the

character of pinning barrier distribution in the material, namely, of the field dependence of the effective pinning barrier  $U_0(B)$ . If  $U_0(B)$  does not vary with temperature,  $n$  is temperature independent and the MHLs scale with temperature and vice versa.

It is shown that the fitting functions due to both the power-law and the logarithmic potential give an equally good fit to the experimental data in RE-123 materials. However, the parameters  $p$  and  $q$  deduced from the experiments on RE-123 samples are well above the values predicted so far by theory, including  $\Delta\kappa$  pinning. Moreover, they strongly fluctuate from case to case and therefore they are hardly suitable for characterisation of pinning regimes in different materials. The exponentially decaying functions  $J(B)$  and  $F(B)$  fit most of the experimental data with only one free parameter, which speaks in favour of the logarithmic potential. However, similarly as for all the classical and modern power-law models, the correspondence between the empirical theory and the microscopic pinning mechanism is still missing.

We hope that the present paper will promote a development of a new pinning theory relevant to the vortex interaction with a random pinning disorder in the high- $T_c$  materials.

## Acknowledgements

This work was partially supported by NEDO for the Research and Development of Industrial Science and Technology Frontier Program. MJ and MRK thank the Japanese Science and Technology Agency (STA) for providing the fellowship. MJ appreciates the support of the Grant Agency of ASCR by the grant A1010919.

## Appendix A

We start from Eq. (14) of Ref. [25] that states

$$F(B) = BJ_0 \left( \frac{E}{E_0} \right)^{kT/F_{p0}V\xi} \quad (\text{A1})$$

By introducing  $b_i = B/B_{\text{irr}}$ ,  $b = B/B_{c2}$ ,  $V = d^3 = \alpha B^{-3/2}$ , and  $F_{p0} = \beta b^\gamma$  ( $\alpha$  and  $\beta$  being field-independent parameters), one receives

$$F(b_i) = R_3 b_i \left( \frac{E}{E_0} \right)^{A b_i^{1.5-\gamma}} \quad (\text{A2})$$

with  $R_3 = J_0 B_{\text{irr}}$  and  $A = kT/(\beta \alpha B_{\text{irr}}^{1.5-\gamma} B_{c2}^\gamma \xi) = \ln(J_{\text{irr}}/J_0)/\ln(E/E_0)$ .  $J_{\text{irr}}$  was defined as a threshold current criterion, above which the pinning force density is negligibly small, and  $(E_0, J_0)$  as the point of  $E$ - $J$  curve taken at the electric field as low as possible. The difference between Eq. (A2) and Eq. (26) in Ref. [25] is evidently due to a misprint in Ref. [25].

The expression (A2) can be also written as

$$F(b_i) = R_3 b_i \exp \left( b_i^{1.5-\gamma} \ln \frac{J_{\text{irr}}}{J_0} \right) \quad (\text{A3})$$

The application of the condition  $\partial F(B)/\partial B|_{B=B_{\text{fp}}} = 0$ , where  $B_{\text{fp}}$  is the position of maximum on the  $F(B)$  curve, gives

$$b_{\text{fi}}^{1.5-\gamma} \ln \frac{J_{\text{irr}}}{J_0} = - \frac{1}{1.5-\gamma} \quad (\text{A4})$$

with  $b_{\text{fi}} = B_{\text{fp}}/B_{\text{irr}}$ .

In terms of  $b_{\text{fp}} = B/B_{\text{fp}}$ , Eq. (A3) reads

$$F(b_{\text{fp}}) = R_3 b_{\text{fi}} b_{\text{fp}} \exp \left[ (b_{\text{fi}} b_{\text{fp}})^{1.5-\gamma} \ln \frac{J_{\text{irr}}}{J_0} \right] \quad (\text{A5})$$

Using the relation (A4), we finally arrive at

$$F_n(b_{\text{fp}}) = b_{\text{fp}} \exp \left( \frac{1 - b_{\text{fp}}^{1.5-\gamma}}{1.5-\gamma} \right) \quad (\text{A6})$$

Similarly, for  $V = d^2\xi$ , Eq. (A6) has the form

$$F_n(b_{\text{fp}}) = b_{\text{fp}} \exp \left( \frac{1 - b_{\text{fp}}^{1-\gamma}}{1-\gamma} \right) \quad (\text{A7})$$

## References

- [1] A.A. Zhukov, H. Küpfer, G.K. Perkins, L.F. Cohen, A.D. Caplin, S.A. Klestov, H. Claus, V.I. Voronkova, T. Wolf, H. Wühl, Phys. Rev. B 51 (1995) 12704.
- [2] A. Erb, J.-Y. Genoud, F. Marti, M. Däumling, E. Walker, R. Flükiger, J. Low Temp. Phys. 105 (1996) 1023.
- [3] H. Küpfer, A.A. Th. Wolf, C. Zhukov, W. Lessing, R. Jahn, Proc. ASMCCD'96, 17–20 September, Mumbai, India, 1996.

- [4] H. K pfer, Th. Wolf, C. Lessing, A.A. Zhukov, X. Lan on, R. Meier-Hirmer, W. Schauer, H. W hl, *Phys. Rev. B* 58 (1998) 2886.
- [5] T. Nishizaki, T. Naito, N. Kobayashi, *Physica C* 282–287 (1997) 2117.
- [6] T. Nishizaki, T. Naito, N. Kobayashi, *Phys. Rev. B* 58 (1998) 11169.
- [7] T. Nishizaki, T. Naito, N. Kobayashi, *Physica C* 317–318 (1999) 645.
- [8] Th. Wolf, H. K pfer, H. W hl, in: T. Matsushita, K. Yamafuji (Eds.), 8th International Workshop on Critical Currents in Superconductors, Kitakyushu, Japan, 27–29 May 1996, World Scientific, Singapore, 1997.
- [9] M. Muralidhar, M.R. Koblischka, M. Murakami, *Supercond. Sci. Technol.* 12 (1999) 555.
- [10] M. Jirsa, M.R. Koblischka, M. Muralidhar, A. Das, M. Murakami, *Advances in Superconductivity* 11 (1) (1999) 243, (Proceedings of the 11th ISS'98, Nov. 16–19, Fukuoka).
- [11] F. Frangi, S.I. Yoo, N. Sakai, M. Murakami, *J. Mater. Res.* 12 (1997) 1990.
- [12] Th. Wolf, A.-C. Bornarel, H. K pfer, R. Meier-Hirmer, B. Obst, *Phys. Rev. B* 56 (1997) 6308.
- [13] T. Egi et al., *Appl. Phys. Lett.* 67 (1995) 2406.
- [14] N. Chikumoto, J. Yoshioka, M. Murakami, *Physica C* 291 (1997) 79.
- [15] B. Khaykovich, E. Zeldov, D. Majer, T.W. Li, P.H. Kes, M. Konczykowski, *Phys. Rev. Lett.* 76 (1996) 2555.
- [16] R.A. Doyle, B. Khaykovich, M. Konczykowski, E. Zeldov, N. Morozov, D. Mayer, P.H. Kes, V. Vinokur, *Physica C* 282–287 (1997) 323.
- [17] W.A. Fietz, W.W. Webb, *Phys. Rev.* 178 (1969) 657.
- [18] E.J. Kramer, *J. Appl. Phys.* 44 (1973) 1360.
- [19] D. Dew-Hughes, *Philos. Mag.* 30 (1974) 293.
- [20] A.M. Campbell, J.E. Evetts, *Adv. Phys.* 21 (1972) 199.
- [21] R.G. Hampshire, M.T. Taylor, *J. Phys. F* 2 (1972) 89.
- [22] G. Antesberger, H. Ullmaier, *Philos. Mag.* 29 (1974) 1101.
- [23] J.N. Li, F.R. De Boer, L.W. Roeland, M.J.V. Menken, K. Kadowksi, A.A. Menovski, J.J. Franse, P.H. Kes, *Physica C* 169 (1990) 81.
- [24] Y. Yeshurun, A.P. Malozemoff, *Phys. Rev. Lett.* 60 (1988) 2202.
- [25] P. Fabricatore, C. Priano, A. Sciutti, G. Gemme, R. Musenich, R. Parodi, F. G m ry, J.R. Thompson, *Phys. Rev. B* 54 (1996) 12543.
- [26] D. Yin, W. Schauer, V. Winde, H. K pfer, S. Zhang, J. Chen, *Z. Phys. B* 94 (1994) 249.
- [27] D. Yin, Ch. Li, W. Bai, *Appl. Supercond.* 5 (1998) 147.
- [28] G.K. Perkins, L.F. Cohen, A.A. Zhukov, A.D. Caplin, *Phys. Rev. B* 51 (1995) 8513.
- [29] G.K. Perkins, A.D. Caplin, *Phys. Rev. B* 54 (1996) 12551.
- [30] M. Jirsa, L. Pust, D. Dlouh y, M.R. Koblischka, *Phys. Rev. B* 55 (1997) 3276.
- [31] M. Jirsa, L. Pust, *Physica C* 291 (1997) 17.
- [32] T. Kobayashi, T. Kimura, J. Shimoyama, K. Kishio, K. Kitazawa, K. Yamafuji, *Physica C* 254 (1995) 213.
- [33] A.A. Zhukov, H. K pfer, S.A. Klestov, V.I. Voronkova, V.K. Yankovsky, *J. Alloy Compd.* 195 (1993) 479.
- [34] C.D. Wei, Z.X. Liu, H.T. Ren, L. Xiao, *Physica C* 260 (1996) 130.
- [35] M. Jirsa, M.R. Koblischka, M. Muralidhar, A. Das, M. Murakami, *Advances in Superconductivity XI*, in: N. Koshizuka, S. Tajima (Eds.), Proceedings of the 11th International Symposium on Superconductivity, November 16–19, 1998, Fukuoka, Japan, Springer-Verlag, Tokyo, 1999, pp. 243–246.
- [36] T. Higuchi, S.I. Yoo, K. Waki, H. Fujimoto, M. Murakami, *Physica C* 282–287 (1997) 2137.
- [37] L. Civale et al., *Phys. Rev. B* 43 (1991) 13732.
- [38] T. Nishizaki et al., *Physica C* 181 (1991) 223.
- [39] L. Klein et al., *Phys. Rev. B* 49 (1994) 4403.